

OPTICAL DIAGNOSTICS IN A SPARK IGNITION ENGINE FOR TWO-WHEEL VEHICLES

Simona Silvia Merola, Paolo Sementa, Cinzia Tornatore

Istituto Motori – CNR

via G. Marconi 8, 80125 Napoli, Italy

e-mail: s.merola@im.cnr.it, p.sementa@im.cnr.it, c.tornatore@im.cnr.it

Abstract

Different optical techniques were applied to describe the thermal and chemical processes that occur in a SI small engine from the ported fuel injection and in-cylinder mixture formation to the combustion process and the exhaust emission. In PFI SI engines, the atomized fuel is sprayed towards the intake valves, where it may evaporate, puddle or rebound. Furthermore, a portion of the fuel may flow directly into the cylinder or impinge upon the port walls. These phenomena occur in varying degrees and depend upon the engine design, injector location and engine operation. Potentially the fuel can enter the cylinder in a poorly atomized state, leading to an increased unburned hydrocarbon emissions. This is particularly true during cold operation, when evaporation is low. In the small-motorcycle and scooter engines the fuel injection occurs in smaller intake manifold than light-duty vehicle engines, increasing the criticism of the fuel-wall interaction. The experimental investigations were performed in a single cylinder engine constituted by an elongated optically accessible piston and equipped with the head and injection system of a reference 4-stroke engine for small vehicles. High spatial resolution imaging was used to characterize the fuel injection phase. The cycle resolved visualization was performed to follow the flame propagation from the intake spark ignition to the exhaust phase. Natural emission spectroscopy measurements were applied in the ultraviolet-visible wavelength range to identify the chemical species that are markers of the combustion process and to follow the formation of pollutants.

Keywords: *spark ignition engine, gasoline, 2-wheel vehicle, optical diagnostics, digital imaging, spectroscopy*

1. Introduction

Motor vehicle ownerships are growing rapidly with a strong impact on air pollution, energy consumption, traffic congestion, accidents, noise, and transport wastes. In emerging countries, the two-wheel and three-wheel vehicles have high diffusion in urban areas due to their higher mobility, more reasonable price, and lower fuel consumption than passenger cars [1-4]. The almost totality of these vehicles are equipped with port-fuel-injected (PFI) spark ignition (SI) engine. In emerging markets, the PFI engine will remain dominant on the more expensive direct injection alternative. Processes in PFI SI engines are reasonably well understood thanks to synergy between the traditional combustion-heat-release analysis, emissions measurements, and quasi-dimensional modelling with the optical diagnostics and CFD analysis. [5-7]. On the other hand, more work should be done in this area for small-motorcycle and scooter engines considering that worldwide emission regulations for two-wheel vehicles are becoming ever more severe [8].

A better understanding of the phenomena connected to the engine combustion process can contribute to the reduction in specific fuel consumption and exhaust emissions is necessary. For example, the fuel storage on the port and on the intake valves puddles determines variations of the air/fuel ratio in engine transient conditions, particularly relevant for light-duty vehicles operating in urban areas. This is very influent on the combustion process, on the pollutant formation and on the effectiveness of post treatment devices, eventually present. Measurement of the in-cylinder processes, particularly within a single-cycle and from one-cycle to the next, does play an important role in the research, modelling and ultimately development of modern PFI engines.

In this work, experimental investigations of fuel injection phase, combustion process and pollutant formation were performed in a port fuel injection spark ignition 4-stroke engine for 2-

wheel vehicle. The engine was equipped with an optically accessible combustion chamber and with the head and injection system of the equivalent commercial engine. High spatial resolution imaging and digital cycle resolved visualization were used to follow the flame propagation from the spark ignition to the exhaust phase. Natural emission spectroscopy in the wavelength range UV-visible allowed the detection of the chemical markers of the combustion process. The effect of fuel injection phasing, number of injections and engine speed were tested.

2. Experimental Apparatus

The optically accessible single-cylinder, PFI, four-stroke SI engine used for the experimental investigations had 72 mm bore, 60 mm stroke and 10 geometric compression ratio. The maximum speed and power of the optical engine were 5000 rpm and 7.9 kW, respectively. The engine was equipped with the four-valve pent-roof head of a commercial 250 cc two-wheel vehicle. The head had a centrally located spark plug and a quartz pressure transducer was flush-installed in the combustion chamber to measure the in-cylinder pressure. A section of the concentric flat-bottomed piston bowl was replaced with a sapphire window to enable the passage of optical signals coming from the combustion chamber. Fig. 1 shows the experimental apparatus used in this work with the optical setup and the bottom field of view of the combustion chamber.

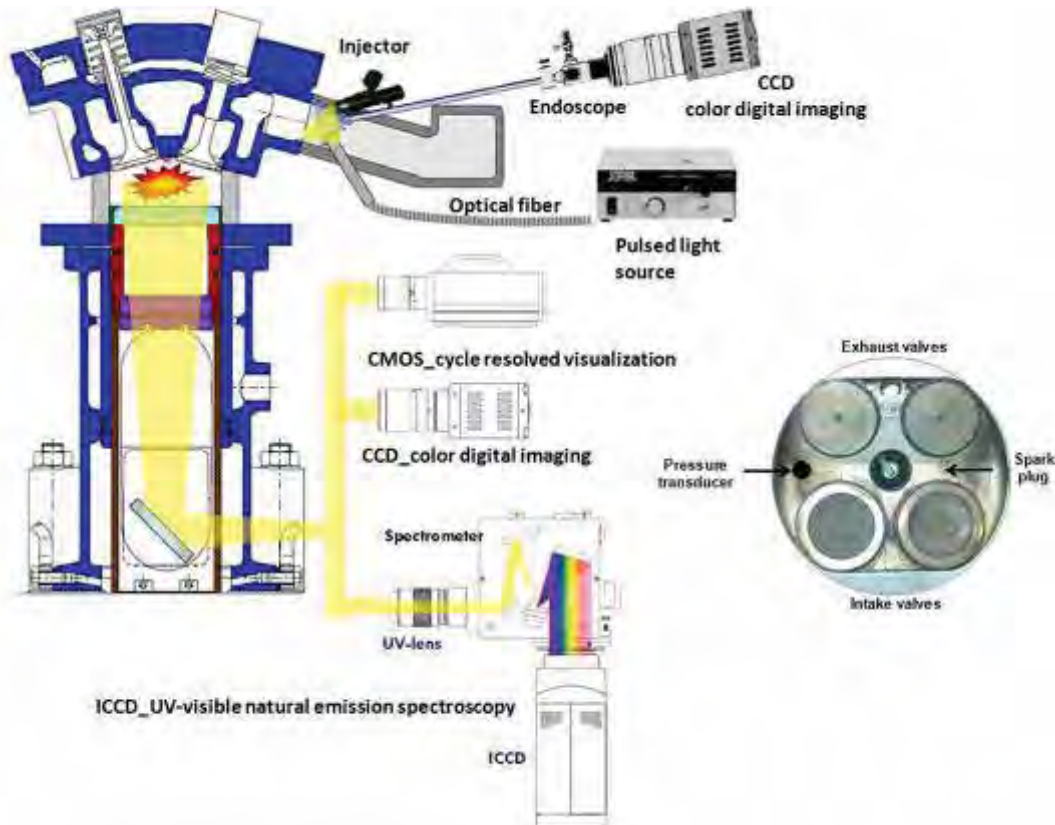


Fig. 1. Experimental setup for optical investigations and bottom field of view of the combustion chamber

The intake manifold was modified and equipped with an endoscopic system coupled with a 12-bit CCD colour camera that mounted a 50 mm focal length, f/3.8 Nikon lens. The CCD had a 640×480 pixel matrix with a pixel size of $9.9 \times 9.9 \mu\text{m}^2$. This optical assessment allowed a spatial resolution around $90 \mu\text{m}/\text{pixel}$. The spectral range of the camera was 300-800 nm. The exposure time was fixed at $55.5 \mu\text{s}$ which corresponds to 1 CAD at an engine speed of 3000 rpm. The dwell time between two consecutive images was $55.5 \mu\text{s}$. The fuel spray was illuminated by flash cold pulsed light source through an optical fibre.

During the combustion process, the radiations emitted passed through the sapphire window and they were reflected toward the optical detection assembly by a 45° inclined UV-visible mirror located at the bottom of the elongated piston. High spatial resolution flame visualization was obtained by a 12-bit digital CCD colour camera with the same specifications of the one used for fuel injection imaging.

For the spectroscopic investigations, a 78 mm focal length, f/3.8 UV Nikon objective focused the light onto the micrometer controlled entrance slit of a spectrometer with 150 mm focal length and 300 groove/mm grating. From the grating the radiations were detected by an intensified cooled CCD camera (ICCD). The ICCD had an array size of 512×512 pixels with a pixel size of 19×19 μm² and 16-bit dynamic range digitization at 100 kHz. The ICCD spectral range spread from UV (180 nm) until IR (800 nm). The match between the spectrometer and the ICCD allowed to simultaneously detect 300 spectra with a spatial resolution along the entrance slit height around 0.18 mm. The dwell time between two consecutive images was set at 55.5 μs. In this work the central wavelength of the grating was fixed at 300 nm and 400 nm in order to cover the spectral range from UV (200 nm) until visible (510 nm). The spectral resolution was 0.49 nm/pixel. The exposure time was fixed at 55.5 μs. The spectroscopic investigations were carried out in the central region of the combustion chamber extended from the intake valves to the exhaust ones. For a better post-detection analysis the binning of 50 spectra was performed in correspondence to four chamber locations. The locations P1 and P2 matched the region around the spark plug; locations I and E corresponded to the region between the intake and exhaust valves, respectively.

Cycle resolved flame visualization was performed by 8-bit high speed camera (512×512 pixel) equipped with a 50 mm focal Nikon lens. The spectral range of the high speed camera extended from 400 nm to 900 nm. A camera region of interest was selected (360×360 pixel) to obtain the best match between spatial and temporal resolution. This optical assessment allowed a spatial resolution around 0.25 mm/pixel and a frame rate of 7188 fps. The exposure time was fixed at 10 μs. The Crank Angle Encoder signal synchronized the cameras and the engine through a unit delay. AVL Indimodul recorded the TTL signal from the camera acquisitions together with the signal acquired by the pressure transducer. In this way, it was possible to determine the crank angles where optical data were detected. The CCD and ICCD were not cycle resolved detectors and each acquisition was performed at different engine cycles.

To reduce the oil contamination of windows, self-lubricating Teflon-bronze composite piston rings in the optical section were used. A special customized lube oil and coolant conditioning unit for transparent single cylinder engine application was used. A lambda sensor was installed at the engine exhaust for the measurement of the air/fuel ratio.

3. Results and Discussion

All the tests presented in this section were carried out at an engine speed of 3000 rpm at wide open throttle. The intake air temperature was fixed at 298 K and the cooling water temperature was set at 333 K. Euro IV gasoline was injected at 3 bar using the standard 3-hole injector. The electronic end of fuel injection was fixed at 60 CAD ATDC. The injection duration was 168 CAD; this allowed reaching the stoichiometric air-fuel ratio as measured by a lambda sensor installed at the engine exhaust. The electronic spark timing was fixed to operate at the maximum brake torque (22 CAD BTDC). The IMEP and COV measured on 400 consecutive cycles were 6.4 bar and 0.9%, respectively. These values were comparable with the real engine. Moreover, the thermal evolution and fluctuation of the maximum pressure signal due to the cyclic variation resulted satisfactory and always lower than 15%. This result demonstrated that the heat transfer among the different components of the optical engine could be considered negligible.

Figure 2 shows a selection of images detected during the fuel injection phase. The first droplets were revealed just before 60 CAD BTDC. The delay with respect to the electronic signal was due to the inertia of the injection system. The injector sprayed part of the fuel towards the plate between

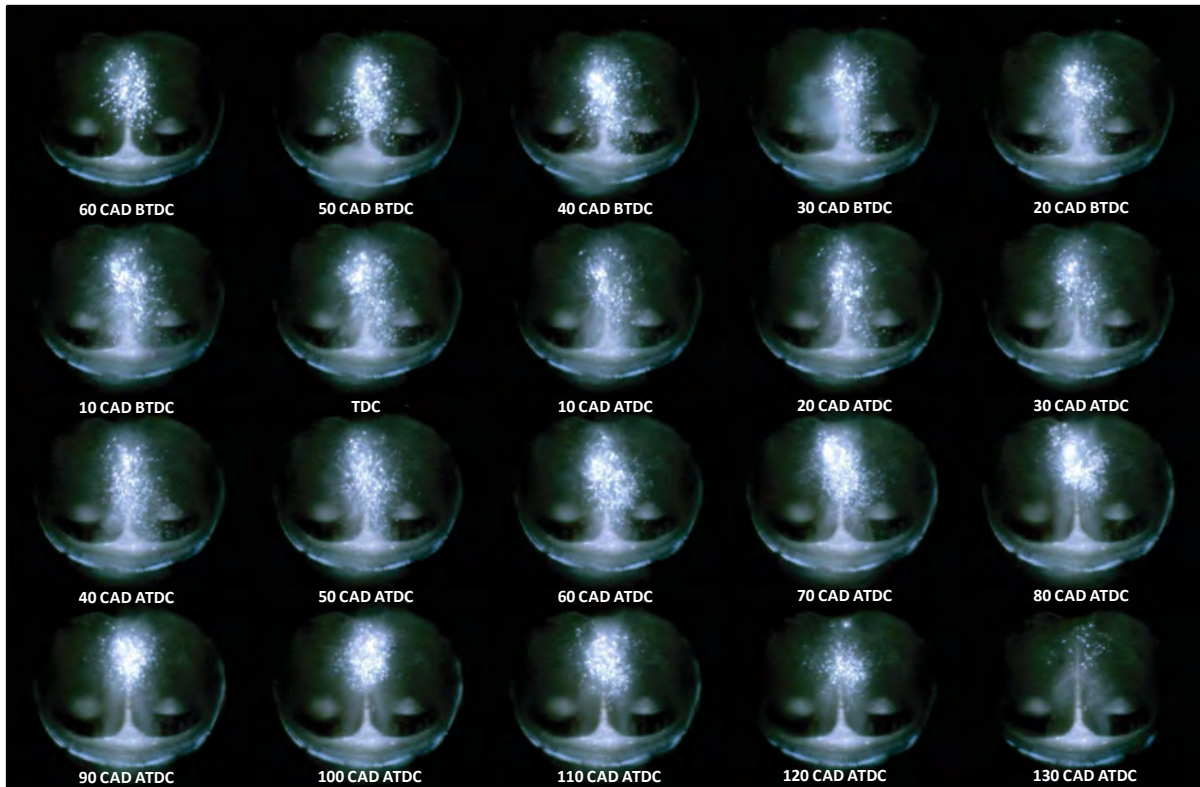


Fig. 2. Images detected in the intake manifold during the fuel injection phase

the intake valves and on the intake valves stems. The droplets impingement induced fuel layer formation on the intake manifold walls. The fuel deposits were drawn by gravity on the valve head where they remained as film due to the surface tension. At TDC, the intake valves lift was around 1 mm and part of the droplets started to pass directly into the combustion chamber by means of the gas flow. The crush of the droplets on the cylinder walls and on the piston surface could take place [9-11].

The fuel film around the valves and the fuel droplets on the combustion chamber walls created fuel-rich zones that developed dynamically under the effect of the gas flow influencing the composition of the mixture and hence the combustion process. To better understand this phenomenon, high spatial resolution imaging of the combustion process was performed. Fig. 3 shows a selection of the flame propagation images detected in the combustion chamber from the spark timing. The evidence of spark ignition was represented by a luminous arc near the spark plug and it occurred around 19 CAD BTDC. The plasma luminosity persisted until 17 CAD BTDC when the flame kernel was observable, even if its luminosity was very lower than the spark. Then flame kernel moved from the spark plug with a radial-like behaviour until around TDC [12]. The flame propagation was influenced by the thermodynamic conditions, the mixture composition and the local turbulence intensity. After TDC, the flame front shape showed an asymmetry: the flame reached first the cylinder walls in the exhaust valves region. This was due to the fuel film deposited on the intake valves that created fuel rich zones in the combustion chamber that slowed down the flame propagation. Moreover, several bright spots were detected in the burned gas before the flame front reached the chamber walls. They were due to the fuel droplets deposited on the sapphire window during the injection when the intake valves were open. These fuel deposits ignited when reached by the normal flame front.

The effect of fuel deposits burning in particular near the intake-valves had strong effect on the late combustion process. Fig. 4 shows the abnormal combustion that took place when the flame front reached the intake valves. The fuel film ignition produced high intensity flame that persisted well after the normal combustion event [13].

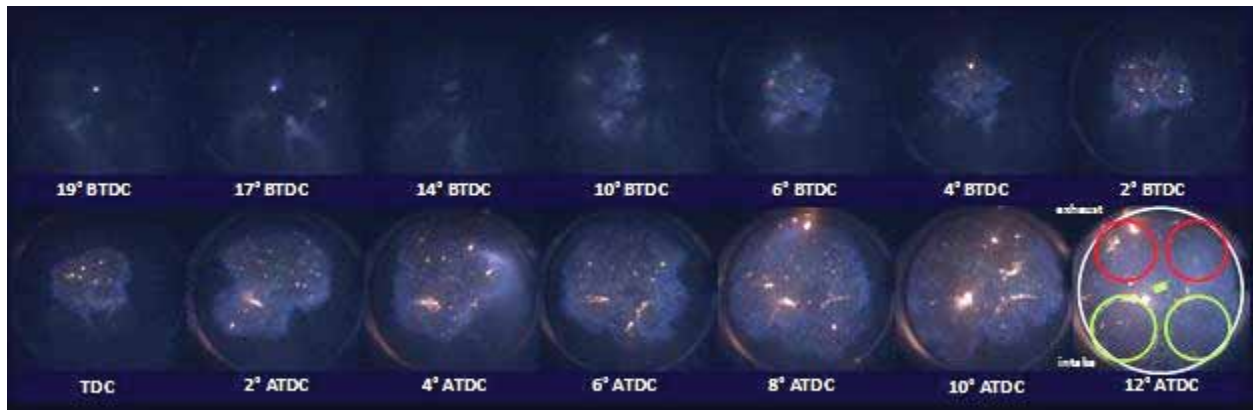


Fig. 3. Images of flame propagation detected in the initial phase of the combustion process

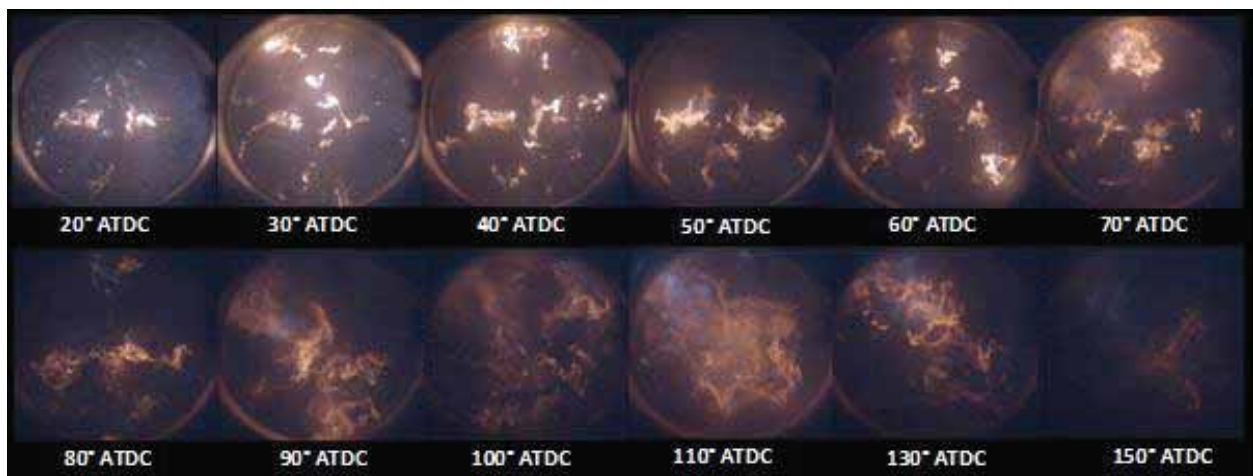


Fig. 4. Images detected during the late phase of the combustion process

To better understand the evolution of the combustion process in terms of chemical species involved in the flame inception and propagation, spectroscopic investigations were carried out. Fig. 5a shows the typical spectra detected at the inception of the spark luminous arc in the locations across the plug (P1 and P2).

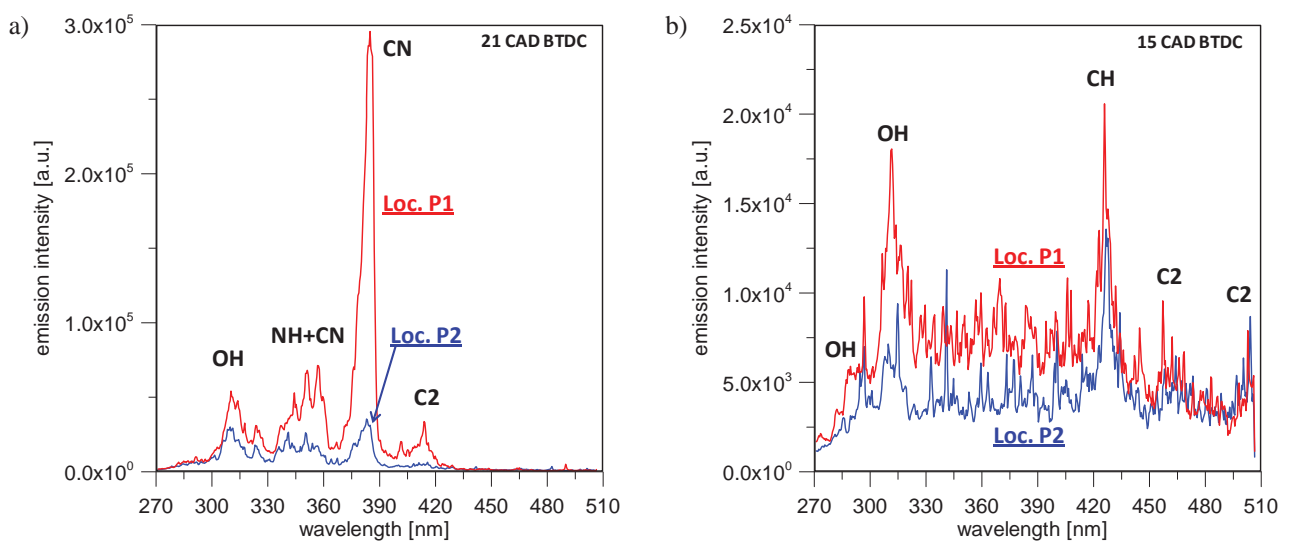


Fig. 5. Typical spectra detected (a) at the inception of the spark luminous arc and (b) at the flame kernel in the locations near the spark plug (P1 and P2)

The interaction between the excited hydrocarbon species and the surrounding air molecules was featured by CN and NH [14, 15]. The presence of CN was outlined by the Violet band system in the spectral range 350 nm - 460 nm. NH shows a very strong emission band around 338 nm and a low intense band around 415 nm. In addition Deslandres - D'Azumbuja C₂ band system was detected around 410 nm. This bands are usually observed under high temperature conditions. An intense head of this system appears at 385.2 nm, but in this case it was masked by the strong CN Violet system. Moreover, OH band system with the highest emission around 309 nm marked the high temperature reactions typical of the plasma at the spark plug [16].

The first evidence of flame emission was detected around 15 CAD BTDC as shown in Fig. 5b. At this time CH and OH radicals were detected [17-19]. CH was featured by three-band system with the strongest band around 431.5 nm. The other one is between 362.8 and 410.0 nm and has closely packed heads; the last band is in the ultraviolet near 315.0 nm and it is usually obscured by OH bands. OH and CH radicals were the markers of the first exothermic reactions, as known by literature [20]. C₂ Swan band system was also detected at 470 nm and 516 nm. C₂ emission was due to the residual of the plasma spark emission. The flame kernel growth consumed the fresh mixture and increased the local gas temperature; thus CH decreased versus OH. The OH and CH features were superimposed on a continuum with two groups of diffuse bands. The first group was due to the Emeleus' bands of formaldehyde molecule CH₂O and it had the highest emission in the range 350-480 nm. The second group identified the Vaidya's bands of HCO with highest heads from 290 nm to 360 nm. Thus the longer wavelength bands were overlapped by the CH₂O and continuum emission.

The relative intensity of the different radiative species evolved but changes in the spectral features were not observed until 3 CAD BTDC. At this time a continuous background related to the carbon monoxide emission was detected (Fig. 6a). High resolution measurements identified carbon monoxide flame bands with closely packed heads in the wavelength range 310-380 nm and 420-490 nm [15, 21].

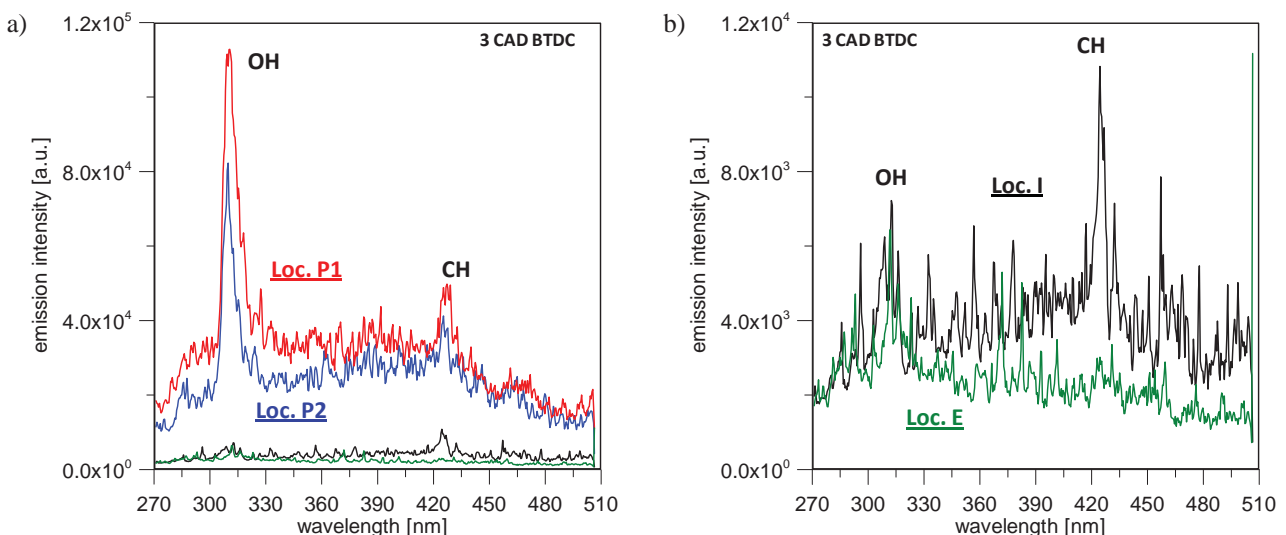


Fig. 6. Typical spectra detected during the flame front propagation in the locations (a) near the spark plug (P1 and P2), (b) between the intake valves (I) and the exhaust valves (E)

Around 3 CAD BTDC, the first evidence of the flame in the location near the exhaust valves (E) and the intake ones (I) occurred too (Fig. 6b). Near the exhaust valves the OH emission and the convolution of HCO and C₂HO emissions were measured, as expected for the premixed combustion. Near the intake valves, CH and broadband contribution maybe due to carbon monoxide bands in the visible wavelength range were detected too. This result was due to the fuel film deposition, already observed by the visualization with high spatial resolution previously reported. In particular,

the well resolved CH band around 431 nm featured the burning of the locally fuel rich-zones near the intake valves. Spectroscopic measurements in the following crank angles showed that the time evolution of CH emission occurred in about 6 CAD. OH emission increased sharply due to the high temperature reactions. Moreover CO-O emission was detected in both the measurement locations. The balance between CH and OH in a reaction zone can be correlated to the local fuel-air ratio evolution.

The flame emission maintained unchanged the spectral behaviour until about 30 CAD ATDC. At this time a broadband signal in the visible wavelength range was detected. This signal evolved in shape and intensity until showing the features of blackbody-like emission (Fig. 7) [15]. This result is due to the diffusion-controlled flames induced by the interaction between the flame front and the fuel film deposit in the combustion chamber. In the final combustion phase the spectral behaviour remained essentially unchanged and only an emission intensity evolution was observed.

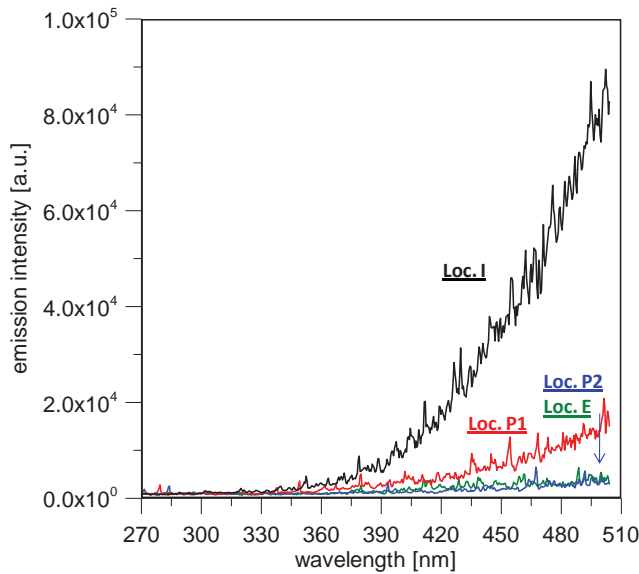


Fig. 7. UV-visible spectra detected in the selected locations at 33 CAD ATDC

Effect of the fuel injection: single and double injection modes

Different fuel injection strategies were tested at 3000 rpm. Initially single injection modes in closed-valve (CV1) and open-valve (OV1) conditions were considered. Then two double injection strategies (DIS) were investigated; they were labelled as OV2 and OV1-CV1. The OV2 had the highest dwell time between the two injections to operate in open-valve condition. The OV1-CV1 was characterised by one injection in closed-valve condition and another one when the intake valves were open. More details about the operating conditions are reported in Tab. 1. The injection-duration was chosen to obtain a stoichiometric equivalence ratio with a coefficient of variation on 400 consecutive cycles lower than 1.8%, as measured by the oxygen sensor at the engine exhaust. The spark timing was always fixed to operate at the maximum brake torque. For all the tests, the values of the averaged IMEP and COV were around 6.4 bar and 0.9%, respectively.

Tab. 1. Engine operating conditions for testing the effect of fuel injection strategies

Test label	N. of Injections	Duration of Inj. [CAD]	Start of Inj. [CAD ATDC]
CV1	1	168	130
OV1	1	172	-300
OV2	2	70, 70	-360, -240
OV1-CV1	2	73, 73	-300, 130

To follow in details the combustion process, cycle resolved imaging of the flame propagation was performed (Fig. 8). For all the tested cases, the first evidence of the flame inception occurred around 2 CAD after the spark ignition. Then the flame front moved from the centrally located spark plug with a radial-like behaviour for about 25-30 CAD. After this time, when the flame reached the intake valves region, the asymmetry in the flame front shape was observed. The flame reached first the cylinder walls in the exhaust valves region due to the fuel film deposited on the intake valves.

As previously discussed, the bright spots in the burned gas were due to the fuel deposits on the sapphire window caused by the strip atomization of the fuel squeezing and fuel droplets sticking. In the open valves condition the effect was enhanced due to the higher number of fuel droplets carried directly into the combustion chamber. The splitting of the fuel injection reduced the number of bright spots that can be considered negligible in the OV1-CV1 condition. This result demonstrated a radical reduction in fuel droplets impingement on the piston surfaces.

The spatial distribution of diffusion-controlled flames was studied through the visualization of the late combustion phase (Fig. 9). In the CV1 condition, highly intense flames were observed near the intake valves, as expected. In the open-valve conditions the flames near the intake valves covered a smaller area. The diffusion-controlled flame luminosity in double injection conditions was lower than in single injection ones and constrained on the intake valve borders. In the OV1-CV1 the flame luminosity was almost negligible just before the exhaust valves opening. This analysis was well supported by the trends of visible flame emission detected in the region between the intake valves and normalised with respect to the maximum of the CV1 emission (Fig. 10).

The spectroscopic investigations previously discussed showed that the diffusion-controlled flames spectra are characterized by the typical spectral feature of the carbonaceous structures and soot. Thus the flame luminosity was correlated to the particulate and HC concentration in the combustion chamber. In this work, the highest soot concentration was obtained in CV1 condition. It was due to the highest fuel deposit amount on the intake-valve stems.

The optical data were in agreement with PM and HC concentration measured at the exhaust by conventional instruments (Tab. 2). It should be noted that the volatile species vaporization from the fuel deposits near the intake valves determined the formation of fuel-rich regions with high density of low-volatile compounds. Thus HC exhaust level was the highest one for CV1 case. The high HC concentration also promoted the soot precursors formation and this is why the CV1 condition showed the highest PM emission. Tab. 2 reports the percentage reduction in BSFC, HC, PM and CO₂ induced by the proposed fuel injection strategies if compared to CV1 condition. To resume, the better fuel-air mixture occurring in the open valve fuel injection strategies (OV) induced higher combustion process efficiency and lower soot production than closed valve strategy (CV). The effect was enhanced by the splitting of the injection (Double Injection Strategies_DIS).

Tab. 2. Percentage reduction in BSFC, HC, PM and CO₂ with respect to the CV1 condition

	BSFC [%]	HC [%]	PM [%]	CO ₂ [%]
OV1	2.9	32.9	40.0	2.9
OV2	1.1	23.1	52.0	1.9
OV1-CV1	3.3	11.2	66.4	6.2

The results gain a more relevant value if they are coupled with CO₂ exhaust emission and with the specific fuel consumption. A significant decrease in CO₂ and BSFC was measured in the double injection strategy OV1-CV1. OV1-CV1 takes advantage of closed valves injection positive aspects without suffering the disadvantages. In OV1-CV1 a portion of fuel is injected when the intake valves are closed, in this way the fuel droplets have enough time to mix with the intake air and a homogeneous mixture can be obtained. The main disadvantage of the closed valves injection

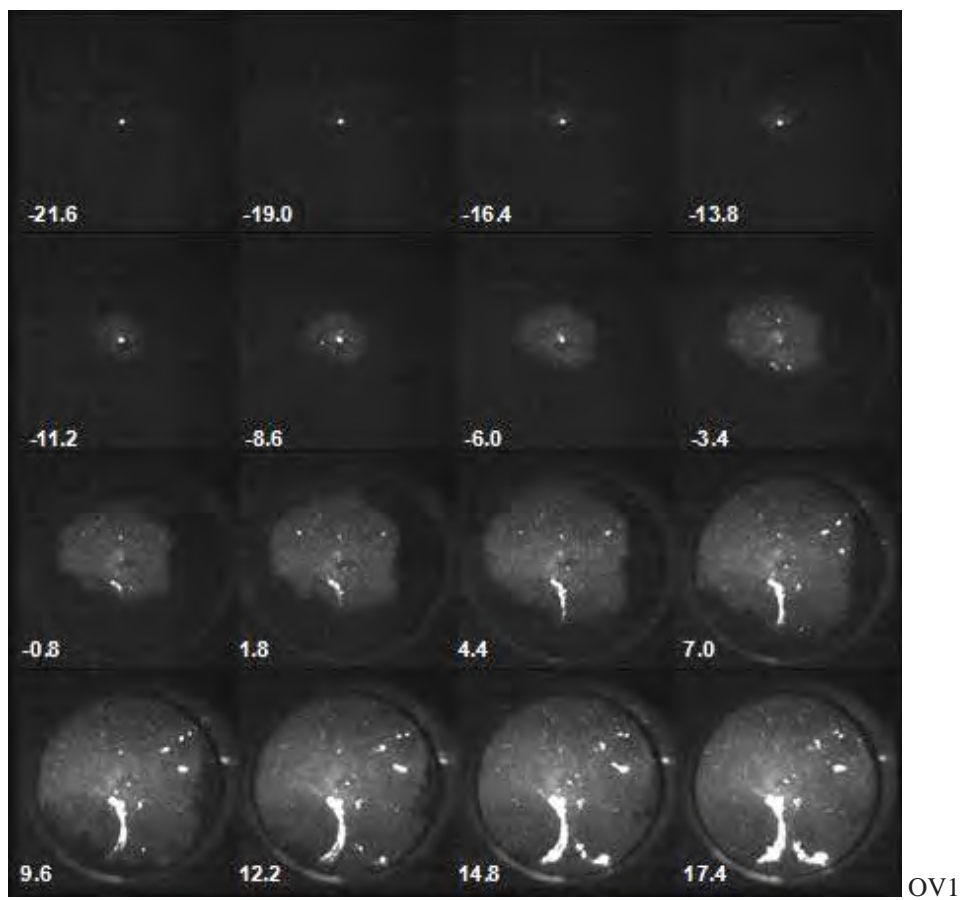
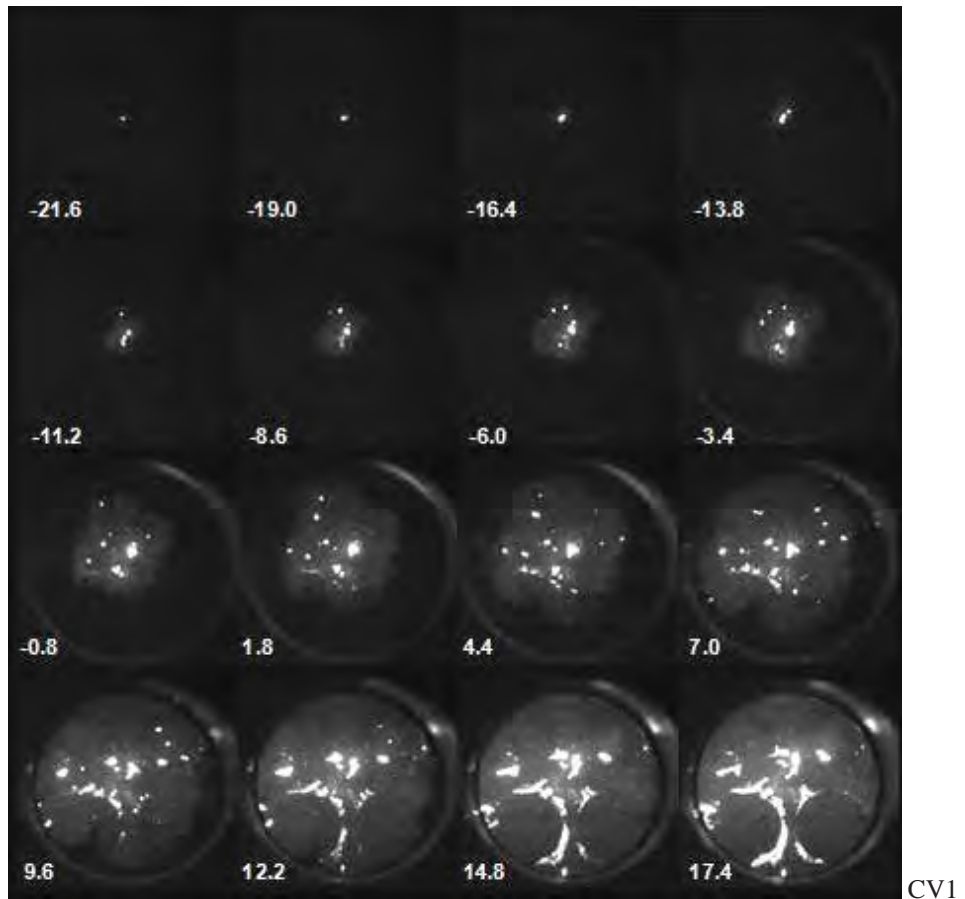


Fig. 8. Cycle-resolved flame propagation for selected injection strategies

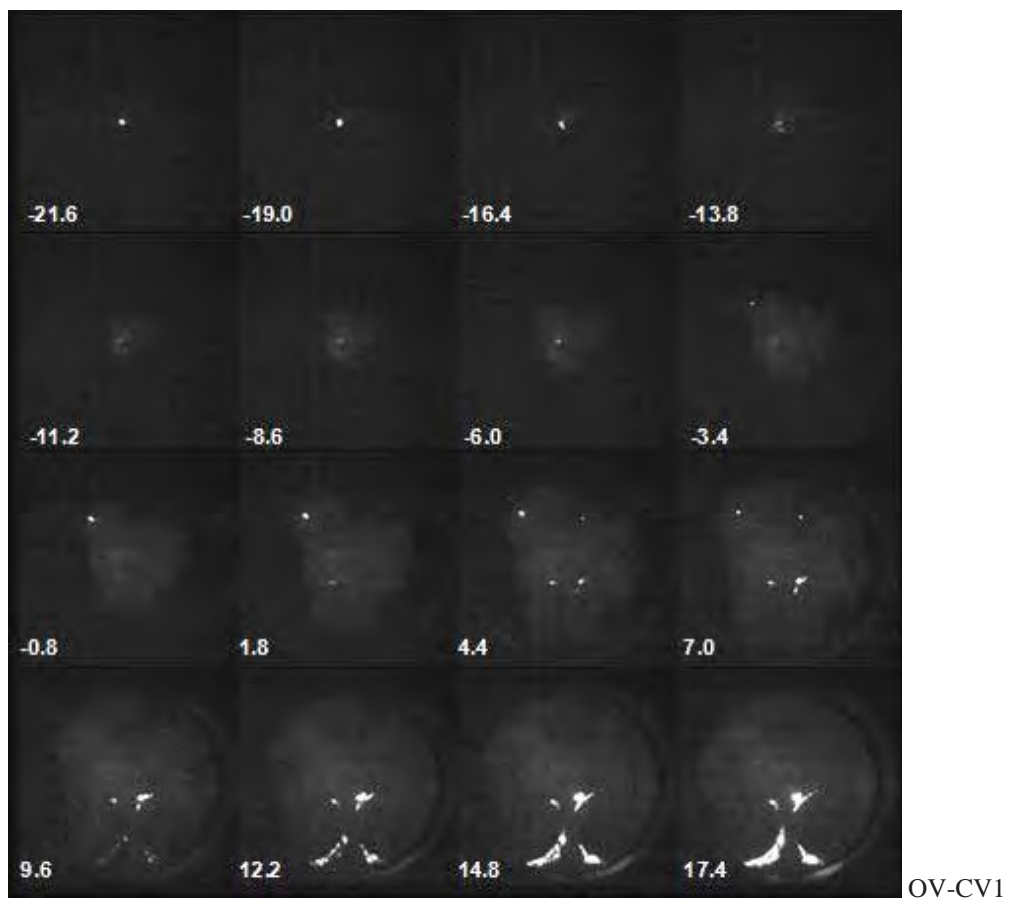
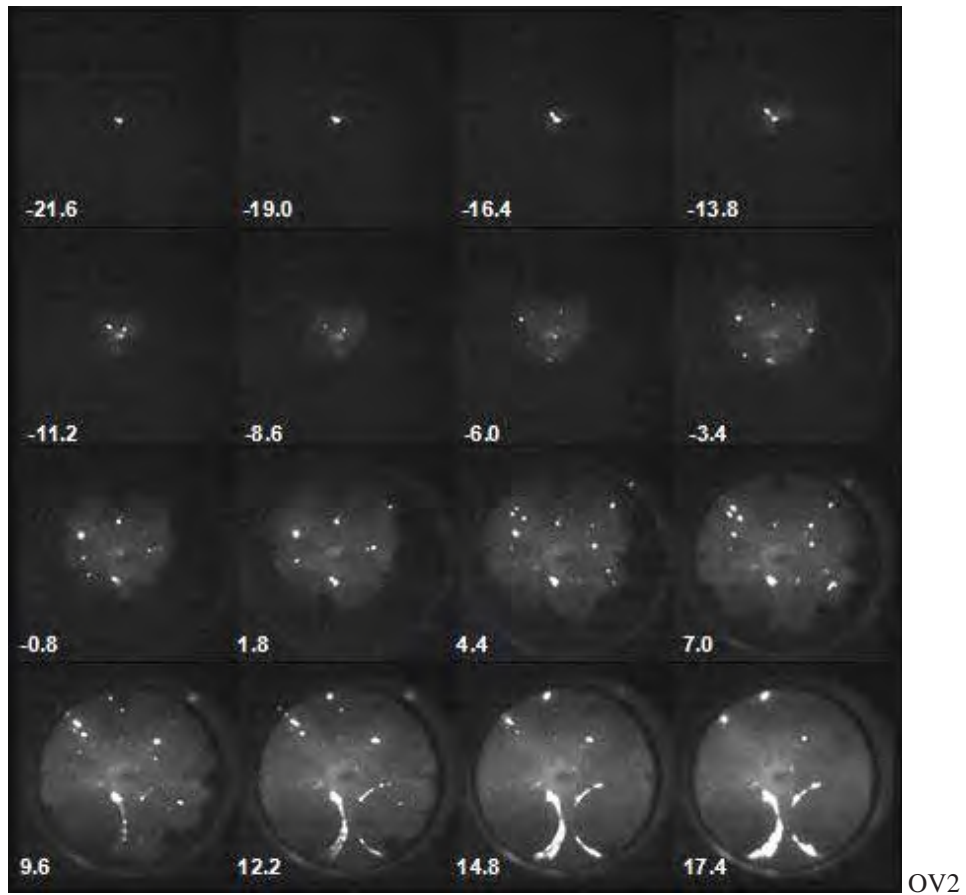


Fig. 8 .Cycle-resolved flame propagation for selected injection strategies (contd.)

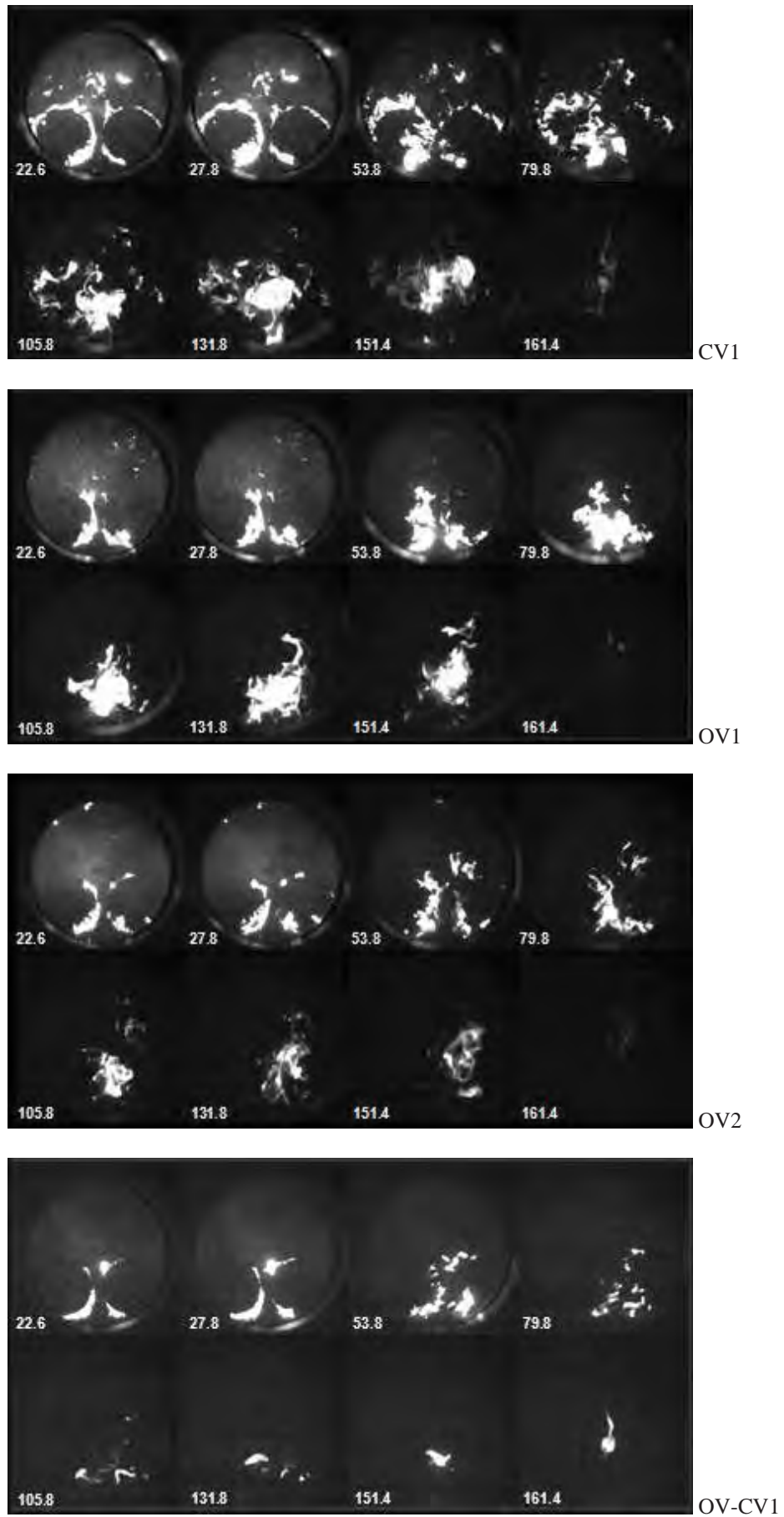


Fig. 9. Cycle-resolved flame propagation in the late combustion phase for selected injection strategies

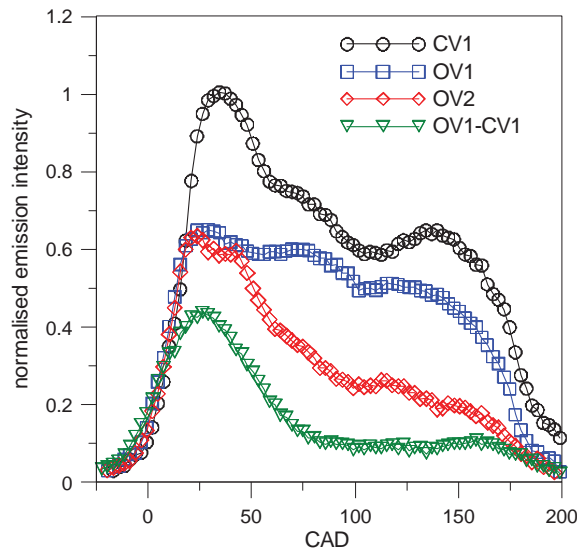


Fig. 10. Visible flame emission detected in the region between the intake valves and normalized with respect to the maximum of the CV1 emission

strategy is the formation of fuel film deposits on the intake ports. In OV1-CV1, there is a small amount of fuel injected when the intake valves are closed: a part of the injection is performed when the intake valves are open. This induces the reduction in pool fire phenomenon. The OV2 condition showed the lowest CO_2 and BSFC reduction percentage; probably because of the valves overlapping. This phenomenon reduced the benefits of injection splitting on the fuel-air mixing.

Effect of the fuel injection and engine speed

Further experiments were realized at 4000 rpm in order to investigate innovative fuel injection strategies as concrete low-cost solution for the optimization of the small engines in terms of pollutant and fuel consumption especially at low speeds and high load. As 3000 rpm cases, the injection-duration was chosen to obtain a stoichiometric equivalence ratio with a coefficient of variation on 400 consecutive cycles lower than 2.0. The spark timing was always fixed to operate at maximum brake torque. For all the tests, the values of the averaged IMEP and COV were around 6.6 bar and 1.4 %, respectively. Tab. 3 reports the details of the tested fuel injection strategies. The only double injection strategy (DIS) was composed by one injection in closed-valve condition and the other in open-valve condition (OV1-CV1). This was the only way to obtain two separated injections considering the injector inertia.

Tab. 3. Engine operating conditions for testing the effect of fuel injection strategies at 4000 rpm

Test label	N. of Injections	Duration of Inj. [CAD]	Start of Inj. [CAD ATDC]
CV1	1	225	0
OV1	1	225	-360
OV1-CV1	2	102, 102	-360, 0

Figure 11 reports the cycle-resolved detection of the flame propagation at 4000 rpm. The number of bright spots in the burned gases is lower than 3000 rpm. It is probably due to the better atomization of fuel spray induced by higher turbulence at 4000 rpm. Moreover at higher engine speed the higher temperature and pressure conditions in the combustion chamber before the spark ignition determined a better vaporization of the fuel deposits near the intake valves. Furthermore, less intense diffusion controlled flames were detected. As a consequence HC, PM and NO_x specific concentration resulted lower at 4000 rpm than 3000 rpm.

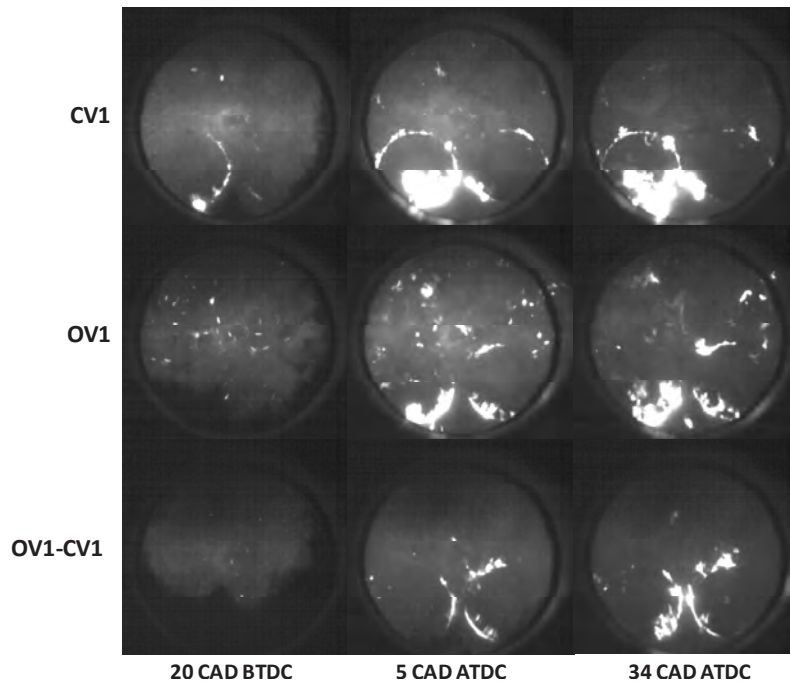


Fig. 11. Selected images from the cycle-resolved detection of the flame propagation acquired at 4000 rpm

About the fuel injection strategies at 4000 rpm, the bright spots in the burned gases were more evident in the OV1 condition than OV1-CV1 and disappeared at the starting of the late combustion phase. The highest intensity of the diffusion-controlled flames near the intake valves was observed in the CV1 condition. In OV1 condition these flames covered a smaller area and they were overall less intense. The diffusion-controlled flame luminosities in double injection conditions were lower than in single injections and constrained on the intake valve borders. In the OV1-CV1 the flame luminosity was almost negligible just before the exhaust valves opening. As measured at lower engine speed, the injection phasing change and the injection splitting induced an overall improvement of the combustion process. Again the highest exhaust PM and HC concentration was obtained in CV1 condition due to the highest fuel deposit amount on the intake-valve stems. It should be noted that the best fuel-air mixture seemed to be obtained for the open valve fuel injection strategy (OV1); in fact, highest performance, stability and lowest CO, CO₂ and specific fuel consumption were measured. At 4000 rpm the advantages of OV1-CV1 condition are not as relevant as for 3000 rpm. At higher engine speed the presence of the second injection in closed valves condition has a negative influence.

4. Conclusions

The effect of fuel injection strategy on the combustion process was investigated by optical diagnostics in a spark ignition 4-stroke engine for 2-wheel vehicles. For all the engine operating conditions, the flame front spread from the spark plug with radial-like behaviour until it reached the intake valves region. Then asymmetry and negative curvature in the flame front outline were observed. This was due to the fuel film deposits formed during the injection process. Intense diffusion-controlled flames were detected especially near the intake valves until the opening of the exhaust valves.

The change of phasing from closed to open valve injection reduced the deposited fuel amount. This effect was improved by the splitting of fuel injection (double injection strategies). As a consequence strong reduction in PM, HC exhaust emission and a reduction in specific fuel consumption were measured.

The proposed options resulted suitable and low-cost solutions for the low speed and full load engine conditions to optimize the combustion process in a spark ignition 4-stroke engine for 2-wheel vehicle.

References

- [1] Han, X., Naeher, L. P., *A review of traffic-related air pollution exposure assessment in the developing world*, Environmental International, Vol. 32, pp. 106-120, 2006.
- [2] Singh, S. K., *Future mobility in India: implications for energy demand and CO₂ emission*, Transport Policy, Vol. 13, pp. 398-412, 2006.
- [3] Vasic, A.-M., Weilenmann, M., *Comparison of real-world emissions from two wheelers and passenger cars*, Environmental Science and Technology, Vol. 40, pp. 149-154, 2006.
- [4] Ntziachristos, L., Mamakos, A., Samaras, Z., Xanthopoulos, A., Iakovou, E., *Emission control options for power two wheelers in Europe*, Atmospheric Environment, Vol. 40, pp. 4547-4561, 2006.
- [5] Maly, R. R., *State of the art and future needs in S.I. engine combustion*, Proceedings of the Combustion Institute, Pittsburgh, USA, Vol. 25 (1), pp. 111-124, 1994.
- [6] Heel, B., Maly, R. R., Weller, H. G., Gosman, A. D., *Validation of S.I. Combustion Model Over Range of Speed, Load, Equivalence Ratio and Spark Timing*, Proceedings of The Fifth International Symposium on Diagnostics and Modeling of Combustion in Internal Combustion Engines (COMODIA 98), pp. 255-260, Tokyo, Japan 1998.
- [7] Drake, M. C., Haworth, D. C., *Advanced gasoline engine development using optical diagnostics and numerical modeling*, Proceedings of the Combustion Institute, Vol. 31 (1), pp. 99-124, 2007.
- [8] <http://www.dieselnet.com/standards/>
- [9] Costanzo, V. S., Heywood, J. B., *Mixture Preparation Mechanisms in a Port Fuel Injected Engine*, SAE Paper No. 2005-01-2080, 2005.
- [10] Gold, M. R., Arcoumanis, C., Whitelaw, J. H., Gaade, J., Wallace, S., *Mixture Preparation Strategies in an Optical Four-Valve Port-Injected Gasoline Engine*, Int. J. of Engine Research, Vol. 1 (1), pp. 41-56, 2000.
- [11] Meyer, R., Heywood, J. B., *Liquid Fuel Transport Mechanisms into the Cylinder of a Firing Port-Injected SI Engine During Start Up*, SAE Paper No. 970865, 1997.
- [12] Merola, S. S., Sementa, P., Tornatore, C., Vaglieco, B. M., *Effect of Fuel Film Deposition on Combustion Process in PFI SI engine*, Journal of KONES Powertrain and Transport, Vol. 14, No. 3, pp. 395-402, 2007.
- [13] Witze, P. O., Green, R. M., *LIF and Flame-Emission Imaging of Liquid Fuel Films and Pool Fires in an SI Engine During a Simulated Cold Start*, SAE Paper No. 970866, 1997.
- [14] Alkemade, C. T. J., Herrmann, R., *Fundamentals of Analytical Flame Spectroscopy*, Hilger eds., Bristol, UK 1979.
- [15] Zizak, G. *Flame Emission Spectroscopy: Fundamentals and Applications*, Lecture given at the ICS Training Course on Laser Diagnostics of Combustion Processes, NILES, University of Cairo, Egypt 2000.
- [16] Dieke, G. H., Crosswhite, H. M., *The ultraviolet bands of OH*, Journal of Quantum Spectrosc. Radiat. Transfer, Vol. 2, pp. 97-199, 1962.
- [17] Gaydon, A. G., Wolfhard, H. G., *Mechanism of formation of CH, C₂, OH and HCO radicals in flames*, Proceeding of Symposium (International) on Combustion, Vol. 4 (1), pp. 211-218, 1953.
- [18] Higgins, B., McQuay, M. Q., Lacas, F., Rolon, J. C., Darabiha, N., Candel, S., *Systematic measurements of OH chemiluminescence for fuel-lean, high-pressure, premixed, laminar flames*, Fuel, Vol. 80 (1), pp. 67-74, 2001.
- [19] Higgins, B., McQuay, M. Q., Lacas, F., Candel, S., *An experimental study on the effect of pressure and strain rate on CH chemiluminescence of premixed fuel-lean methane/air flames*, Fuel, Vol. 80 (11), pp. 1583-1591, 2001.
- [20] Baulch, D. L., Cobos, C. J., Cox, R. A., Esser, C., Frank, P., Just, T., Kerr, J. A., Pilling, M. J., Troe, J., Walker, R. W., Warnatz, J., *Evaluated Kinetic Data for Combustion Modelling*, J. Phys. Chem. Ref. Data, Vol. 21 (3), pp. 411-734, 1992.
- [21] Bessler, W. G., Schulz, C., Lee, T., Jeffries, J. B., Hanson, R. K., *Carbon dioxide UV laser-induced fluorescence in high-pressure flames*, Chemical Physics Letters, Vol. 375 (3-4), pp. 344-349, 2003.